2025 IEEE/AIAA Transportation Electrification Conference and Electric Aircraft Technologies Symposium (ITEC+EATS) | 979-8-3315-2214-8/25/$31.00 ©2025 IEEE | DOI: 10.1109/ITEC63604.2025.11098034

Mission-level Assessment of Environmental Control System Electrification on Hybrid-Electric Turboprop Regional Aircraft

Sijian Tan*, Yu Cai*, Jiacheng Xie*, and Dimitri N. Mavris*
*School of Aerospace Engineering
Georgia Institute of Technology, Atlanta, Georgia 30332–0150
Email: stan43@gatech.edu

***Abstract*—Electrified Aircraft Propulsion (EAP) is gaining significant attention as a potential solution for reducing fuel consumption and emissions. Although electrifying the propulsion system has been a primary focus in past studies, secondary power subsystems such as the environmental control system (ECS) also consume a significant amount of energy, yet their impacts on aircraft mission performance have not been investigated with EAP. This paper presents a parametric modeling approach for the ECS and its electrification on a previously established regional turboprop EAP vehicle model. Semi-empirical and physics-based approaches are used to determine the component weights, drag penalty, and secondary power offtake of ECS. Both the engine-driven generators and the main battery in the EAP system are considered as candidate power source for the electrified ECS. A retrofit study at the vehicle level predicts that electrified ECS architectures bring a 0.4% increase in the empty weight, up to 3% fuel saving at 180 nmi, and a small range reduction of up to 5 nmi.**

***Index Terms*—electrified aircraft propulsion, environmental control system, secondary power, aircraft performance**

I. Introduction

Electrified Aircraft Propulsion (EAP) concepts are increasingly recognized as innovative solutions for the sustainable future of the aerospace industry. There are three primary implementations of EAP: all-electric, turbo-electric, and hybrid-electric propulsion architectures. Compared to the all-electric configuration, the hybrid-electric architecture has a lower weight penalty due to reduced battery requirements [1], [2]. Numerous studies on electrified aircraft propulsion systems have been conducted, providing comprehensive insights into power source and thrust generation architecture [3]–[6]. In addition to propulsion system analysis, evaluating the performance of critical subsystems is crucial to ensure the overall efficiency, safety, and operational reliability of electric aircraft [7], [8]. Among various subsystems, the Environmental Control System (ECS) is responsible for cabin pressurization, temperature control, air ventilation, and humidity control, especially at high altitudes [9], [10]. As the largest power consumer within the aircraft secondary power system, ECS can significantly affect the aircraft's weight and energy consumption [11]. Since the performance of electrified aircraft is more weight-sensitive compared to conventional fuel-only aircraft and electrified subsystems tend to increase the vehicle empty weight [7], it is necessary to explore the trade-off between weight penalty and vehicle mission performance such as fuel consumption, battery energy consumption, and range capability, with subsystem electrification. In the following sections, this paper describes the modeling approach of a conventional pneumatic ECS and an electrified ECS, then analyzes the performance trade-off between three candidate ECS architectures accounting for their power sources.

II. Modeling of Environmental Control System

To maintain the target temperature and pressure inside the aircraft cabin, the aircraft ECS needs to provide a certain amount of fresh air (i.e., supply air). This study considers two types of ECS based on the secondary power they consume: pneumatic ECS and electric ECS. The primary difference is the source of supply air: the pneumatic ECS utilizes bleed air extracted from engine compressors, while the electric ECS employs electrically powered compressors to pressurize ram air as the supply air, eliminating engine bleed air extraction, as shown in Fig. 1. In both types of ECS, the supply air passes through pneumatic air conditioning kits (packs) where its pressure and temperature are regulated by ram air. The conditioned air is then mixed with recirculated air and distributed through ducts to provide ventilation, temperature control, and cabin pressurization.

A. Estimation of Supply Air Mass Flow Rate

The supply air mass flow rate, $\dot{m}_{\mathrm{sup}}$, is a common parameter in sizing and performance evaluation of both pneumatic and electric ECS. Except during takeoff when the ECS is temporarily turned off, the supply air mass flow rate must satisfy the following three criteria, each of which sets a lower bound. The actual mass flow rate is then determined as the highest value among the three.

1) Regulatory requirement: According to the FAA's Advisory Circular AC 25-20 [12], a minimum of $0.55\,\mathrm{lb/min}$ of fresh air per occupant is required during operation to ensure that cabin air quality meets health standards.

2) Air refresh interval: The ECS must be able to renew the cabin air within a certain time interval, assumed to be $2\,\mathrm{min}$ in this study. The estimation of the total mass of cabin air takes into account a cabin pressurization schedule as shown in Fig. 2 (based on Ref. [13]), a constant cabin temperature of $24\,^{\circ}\mathrm{C}$, and the fuselage and cabin geometry.

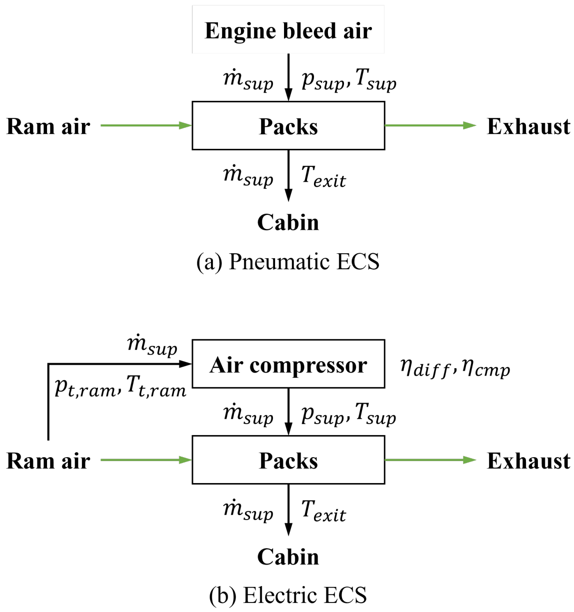

Fig. 1. Schematics of air flow in the pneumatic ECS and the electric ECS

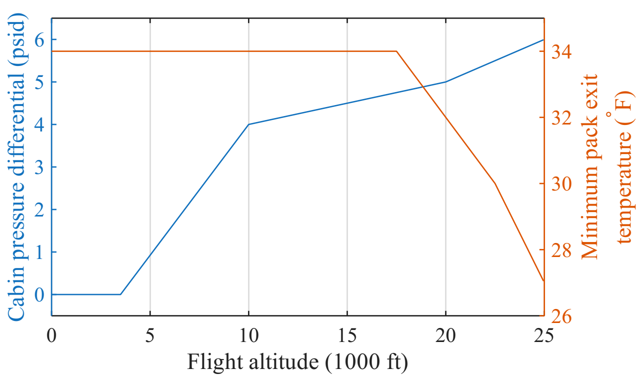

Fig. 2. Cabin pressurization schedule and minimum pack exit temperature

3) Cabin thermal balance: The ECS must be able to maintain cabin thermal balance by pumping supply air at a regulated temperature, also known as the pack exit temperature, T_{exit}. With a constant cabin temperature, cabin thermal balance requires the following:

$$\dot{Q}_{\text{gen}} + \dot{Q}_{\text{wall}} + \dot{Q}_{\text{ECS}} \equiv 0 \tag{1}$$

where a positive value of $\dot{Q}$ implies heat generated inside or flowing into the cabin and a negative value implies heat rejected from the cabin. $\dot{Q}_{\text{gen}}$ is the heat generated by various sources as summarized in Fig. 3 (generated from data in Refs. [14], [15]). $\dot{Q}_{\text{wall}}$ is the heat transferred through the cabin wall and the fuselage skin, estimated based on Muller et al. [14], taking into account cabin temperature, cabin and fuselage geometry, and ambient condition. $\dot{Q}_{\text{ECS}}$ is the cooling power of the supply air, which is determined by the supply air mass flow rate, the air specific heat capacity, the pack exit temperature, and the cabin temperature. A notional altitude-

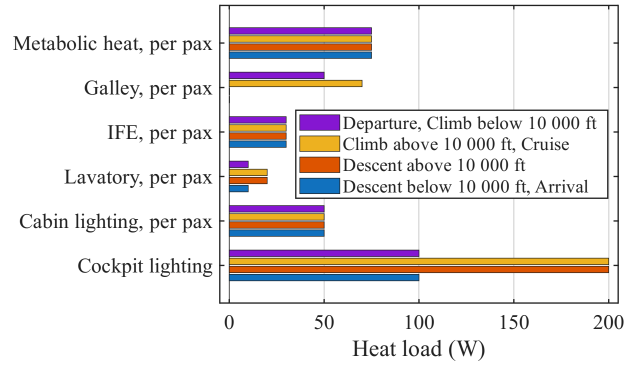

Fig. 3. Summary of cabin heat loads

dependent minimum pack exit temperature schedule as shown in Fig. 2 dictates a minimum supply air flow rate required to maintain cabin thermal balance.

B. Pneumatic ECS Modeling

1) Estimation of Secondary Power Requirement: The pneumatic ECS consumes bleed air as the secondary power extracted from the engine compressors. Assuming no leakage in the pneumatic system, the required bleed air flow rate is equal to the supply air mass flow rate as determined in Sec. II-A.

2) Estimation of Mass: The pneumatic ECS primarily consists of two packs and associated ducts and valves. In this study, a pack model is not explicitly developed. The total mass of the pneumatic ECS is estimated using the empirical relation in NASA Flight Optimization System (FLOPS) software [16].

3) Estimation of Drag Penalty: The pneumatic ECS generates ram drag as it admits ambient air through the packs for cooling purpose. In this study, without a detailed pack model, the drag penalty of the pneumatic ECS is not explicitly evaluated. Instead, its drag penalty is assumed to be included in the drag polar of the baseline model, which is estimated using the Empirical Drag Estimation Technique [17] as a module in FLOPS.

C. Electric ECS Modeling

1) Estimation of Secondary Power Requirement: In electric ECS, the cabin air compressors (CACs) consume electric power and convert it into mechanical power to pressurize the ram air. Given the required supply air mass flow rate $\dot{m}_{\text{sup}}$, flight altitude, airspeed, and compressor discharge pressure schedule as shown in Fig. 4 (reproduced based on Ref. [18]), the mechanical power requirement is estimated as the rate of work done on the ram air to raise its total temperature from the ambient total temperature to the CAC exit, assuming a diffuser efficiency of $90\,\%$ and a compressor mechanical efficiency of $85\,\%$. The electric power requirement additionally accounts for the efficiency of electric motor and power electronics, assumed to be $90\,\%$ and $95\,\%$, respectively.

2) Estimation of Mass: The proposed electric ECS model also consists of two packs, which are supplied by three CACs. Each CAC is sized for $50\,\%$ of the maximum total supply air

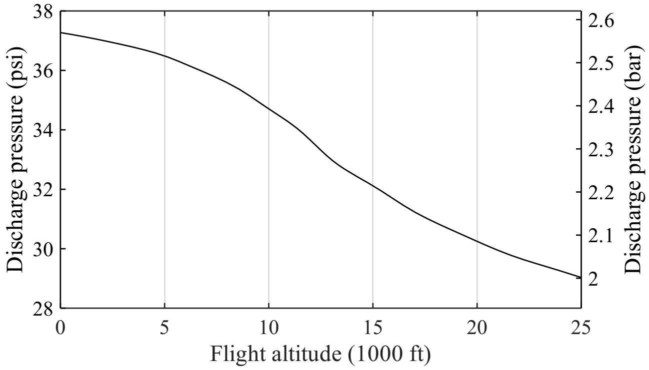

Fig. 4. Cabin air compressor discharge pressure schedule

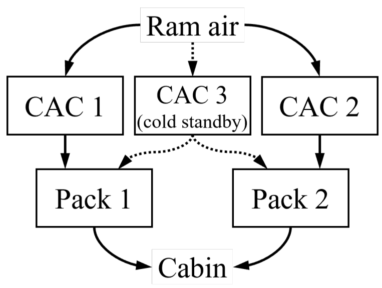

Fig. 5. Electric ECS configuration with a redundant cabin air compressor

flow, allowing one of them to serve as a cold standby for redundancy, as shown in Fig. 5. Each CAC primarily consists of a mechanical compressor, an electric motor, and power electronics, whose masses are estimated based on the sizing power and the power-to-mass ratio, assumed to be $2.5\,\mathrm{kW/kg}$, $13.2\,\mathrm{kW/kg}$ [19], and $13.8\,\mathrm{kW/kg}$ [20], respectively. In this study, it is assumed that the total mass of packs, ducts, and valves remain the same as those of the pneumatic ECS.

3) Estimation of Drag Penalty: The drag penalty of the electric ECS can be decomposed into the ram drag due to pack cooling air and the ram drag due to supply air. In this paper, the ram drag due to pack cooling air is assumed to be the same as in the pneumatic ECS. The ram drag due to supply air is estimated based on a complete loss of momentum, depending on the mass flow rate and the airspeed, as the air is admitted at the CAC inlets.

III. Aircraft Performance Evaluation

A. Propulsion and Subsystem Architectures

This study employs a parallel hybrid-electric propulsion system developed in previous work [21]. As shown in Fig. 6, the hybrid propulsion system is equipped with a pneumatic port for bleed air extraction and an accessory gearbox for shaft power extraction in each of the two gas turbine engines. Electric power can be obtained through the engine-driven generators and/or the power converters connected directly to the battery bus. This propulsion architecture, therefore, offers three candidate subsystem architectures considering the type of ECS and the power source of ECS, as summarized in Table I.

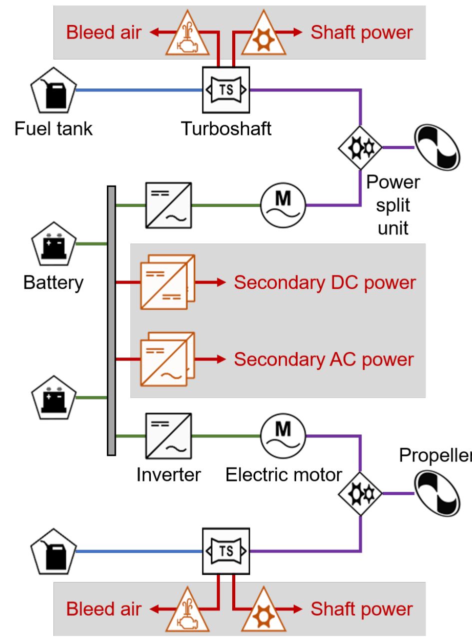

Fig. 6. Proposed parallel hybrid-electric architecture

TABLE I
Candidate Subsystem Architectures

Architecture	ECS Type	ECS Power Source
P-ECS	Pneumatic	Engine bleed
S-ECS	Electric	Engine shaft
B-ECS	Electric	Main battery

B. Baseline Vehicle Model and Analysis Setup

A notional regional turboprop aircraft model based on the ATR 42-600 established in previous work [3] serves as the baseline aircraft model in this study. The baseline model is equipped with the conventional P-ECS architecture, and its high-level characteristics are summarized in Table II, where the power split indicates the fraction of propulsive power supplied by both electric motors, and the block energy consumption accounts for both fuel burn (using a specific energy of $43.2\,\mathrm{MJ/kg}$) and net change of battery energy.

TABLE II
Baseline Vehicle Specifications

Metric	Value
MTOW	$18\,600\,\mathrm{kg}$
OEW including battery	$12\,784\,\mathrm{kg}$
Battery size	$448.5\,\mathrm{kWh}$
Design payload	48 pax $\times$ $95\,\mathrm{kg}$
Range at design payload	$200\,\mathrm{nmi}$
Engine takeoff power	$1338\,\mathrm{kW}$
Electric motor rated power	$271.6\,\mathrm{kW}$
Takeoff power split	$16.9\,\%$
Cruise altitude	$25\,000\,\mathrm{ft}$
Mission performance at 180 nmi	
Block fuel	$491.3\,\mathrm{kg}$
Block energy	$22.20\,\mathrm{GJ}$
Cruise power split	$23.82\,\%$

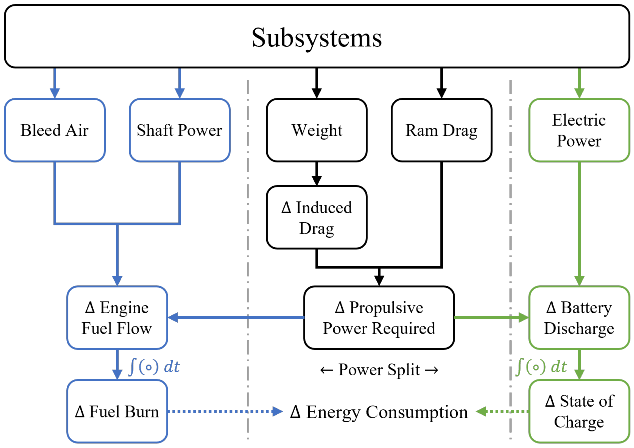

Fig. 7. Propagating subsystem-level impacts to vehicle level

A vehicle retrofit study is conducted to evaluate the performance of electrified subsystem architectures, S-ECS and B-ECS. The maximum takeoff weight (MTOW), geometry, propulsion system, and battery size remain unchanged. An economy mission at a distance of $180\,\mathrm{nmi}$ is used to evaluate the overall impacts on fuel and energy consumption.

C. Capturing Subsystem Impacts at Vehicle Level

In order to evaluate the vehicle-level impacts of ECS electrification, the subsystem power requirements, mass contribution, and drag penalty must be propagated to other vehicle-level analysis modules in the modeling and simulation environment. This is done by implementing the analysis flow shown in Fig. 7.

1) Changes in the subsystem hardware mass (or equivalently, weight) directly impact the vehicle operating empty weight (OEW).
2) The direct weight impacts are captured by the aerodynamic module and affect the lift-dependent drag.
3) The changes in both the lift-dependent drag and the direct drag penalty (such as the ram drag) affect the propulsive power requirement and, subsequently, the rate of consumption of energy sources, namely the fuel flow and the battery output power.
4) Bleed air and shaft power offtake are passed to the engine model, which is established using the Numerical Propulsion System Simulation (NPSS) software [22], to evaluate the incremental fuel penalty.
5) The electric power offtake from the main battery is added directly to the battery output power to update the state of charge.

D. Modeling and Simulation Environment

The vehicle model, the propulsion architecture, and all ECS architectures are implemented in the Modular Aircraft Design Environment (MADE) [3], [15]. MADE is a MATLAB-based, object-oriented, multi-disciplinary analysis and optimization environment developed at Georgia Tech Aerospace Systems Design Laboratory for overall aircraft design and performance analysis. It is able to parametrically model both conventional and electrified propulsion systems and secondary power subsystems. Within MADE, the gas turbine engine model is established in NPSS, the baseline OEW breakdown and drag polar are computed using FLOPS, the integration of subsystem is implemented in custom codes, and an energy-based mission analysis is employed to evaluate a design candidate's mission performance.

IV. Results and Discussions

A. Drag Penalty

Fig. 8 compares the drag penalty, fuel consumption, and battery output power between the three ECS architectures at different flight phases of an economical mission. The range of this economical mission is set at $180\,\mathrm{nmi}$, and the payload is set at the design payload. To provide a flight condition reference for the comparison, Fig. 8 (a) shows the equivalent airspeeds and altitudes where the aircraft flies at different mission phases.

Fig. 8 (b) shows the additional drag introduced by the electrification of ECS compared to the P-ECS. As discussed in Sec. II-C3, such a difference is caused by the ram drag due to supply air, which is determined based on the mass flow rate and the airspeed. Because S-ECS and B-ECS have the same supply air mass flow rate and airspeed during the entire mission, their drag penalties are the same. When the aircraft climbs below $10\,000\,\mathrm{ft}$, the drag penalty decreases due to the decrease in air density. The rapid increase in the drag penalty when crossing $10\,000\,\mathrm{ft}$ is caused by the increase in the heat loads, as shown in Fig. 3. Then, the drag penalty continues to decrease due to the air density change until $25\,000\,\mathrm{ft}$ where another rapid increase occurs. This increase is mainly due to the acceleration, which increases the momentum loss of the ram air. During the cruise, the drag penalties of electric ECSs are about 0.34% compared to P-ECS. The sudden drop of the drag penalty at the top of the descent is due to the reduced heat loads generated by the galley, lavatory, and cockpit lighting. The following variation of the drag penalty during the descent segment is due to the changes in altitude and airspeed.

B. Total Fuel Flow

Fig. 8 (c) presents the total fuel flow rate during the mission when the aircraft is equipped with three types of ECS architectures. It is seen that at altitudes below $10\,000\,\mathrm{ft}$, the aircraft equipped with P-ECS exhibits higher fuel consumption during the climb. This is primarily because, at lower altitudes, the turboshaft engines operate at their maximum torque limit. To maintain the required shaft power while compensating for the increased bleed air extraction, additional fuel is needed. In contrast, when the aircraft climbs at high altitudes, the turboshaft engine operates at its thermal limit (i.e., the maximum turbine entry temperature), rather than the torque limit. Under this condition, extracting bleed air does not require additional fuel to maintain shaft power. As a result, the fuel flow for the P-ECS architecture decreases at higher altitudes.

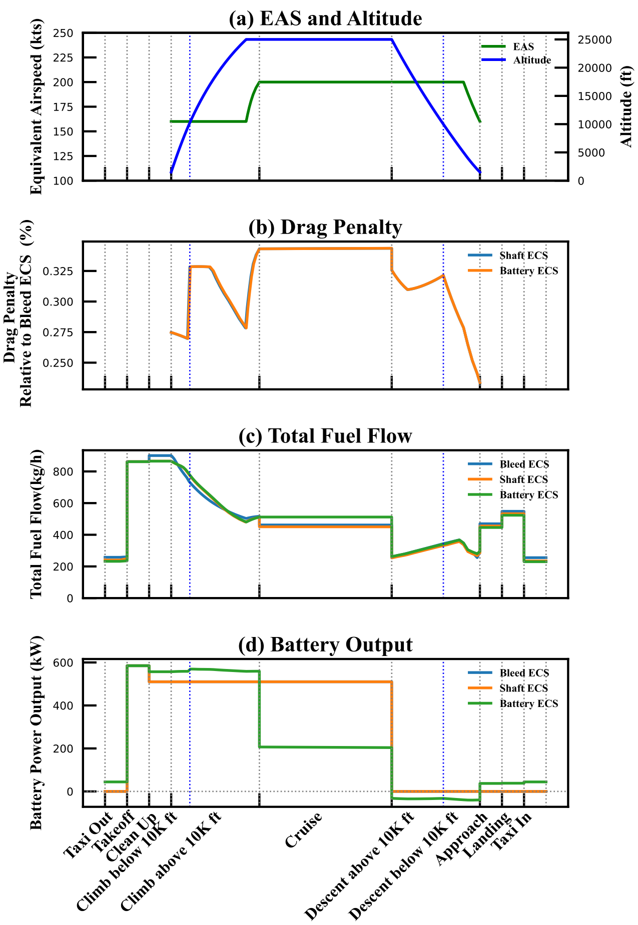

Fig. 8. History diagrams of performance metrics for 180-nmi mission

During the cruise segment, the B-ECS architecture presents a higher fuel flow compared to the other two architectures. This is mainly due to the reduced cruise power split, as shown in Table III. Given the fixed size of the battery, since a part of the battery power needs to allocate to the ECS, the cruise power split has to be decreased to limit the electric power given to propulsion. To compensate and maintain the required propulsive power, the turboshaft engine must operate at a higher power setting, leading to increased fuel consumption.

C. Battery Power Output

Fig. 8 (d) displays the battery power output throughout the mission. As a result of power split optimization [23], the P-ECS and the S-ECS architectures have nearly identical climb and cruise power splits. Since the power splits are optimized for minimum fuel consumption, electric motors operate at their maximum power setting during climb and cruise for both P-ECS and S-ECS. Therefore, the battery power output remains constant from climb to cruise, and the curves for P-ECS and S-ECS overlap in the figure.

On the other hand, the B-ECS architecture shows a higher battery power output during climb. This is because the battery needs to provide power not only to the electric motors, which also operate at maximum power, but also to the ECS. However, during the cruise, the reduced power split for B-ECS limits the propulsive power demanded from the battery. Therefore, the battery output power rapidly drops once the cruise begins. Since the battery is not resized, in-flight recharging is required during descent to increase the stored battery energy at the bottom of descent in order to satisfy the reserve mission requirement [3]. This results in negative net battery power output during descent in Fig. 8, and implies that the ECS is actually powered by engine shaft power instead.

TABLE III
MISSION PERFORMANCE METRICS COMPARISON

Metric	Shaft Power ECS	Battery ECS
Δ OEW	+43 kg (+0.37 %)	+43 kg (+0.37 %)
Δ Block Fuel	−15.2 kg (−3.10 %)	−12.8 kg (−2.61 %)
Δ Block Energy	−627 MJ (−3.29 %)	−666 MJ (−3.00 %)
Cruise Power Split	23.85 %	7.35 %
Δ Range at design payload	−3.4 nmi	−4.8 nmi

D. Overall Mission Performance

Table III summarizes the vheicle-level impacts of ECS electrification. Both S-ECS and B-ECS architectures show a consistent increase of 0.37 % in OEW, which is primarily due to the addition of cabin air compressors. The S-ECS architecture eliminates bleed air offtake and improves overall engine efficiency, resulting in a fuel saving of 3.10 %. Meanwhile, the B-ECS architecture requires additional energy conversion during descent due to the required in-flight recharging, resulting in a less advantageous fuel saving of 2.61 %. Switching the ECS power source from the engines to the main battery also affects the power distribution in the propulsion system, as indicated in the significant decrease in the cruise power split. Analysis also shows a slight range reduction of 3.4 nmi for S-ECS and 4.8 nmi for B-ECS accounting for the net impact of weight, drag, and secondary power offtake. This implies that a resizing or re-optimization at the propulsion or vehicle level is necessary to retain the baseline range capability.

V. CONCLUSION

This paper presents a high-level modeling approach for both the conventional pneumatic ECS and the electrified ECS, followed by vehicle retrofit and a mission-level performance assessment of ECS electrification on a 50-passenger regional turboprop aircraft featuring a parallel hybrid-electric propulsion architecture. Key performance parameters, including component weight, secondary power offtake, and drag penalty, are evaluated at the subsystem level and propagated to the vehicle level through weight build-up, aerodynamic analysis, and propulsion model. Three ECS architectures are evaluated: pneumatic ECS powered by engine bleed air, electric ECS powered by engine-driven generators, and electric ECS powered directly by the main battery in the hybrid propulsion system. As the baseline vehicle is retrofitted with the electrified

ECS architectures, the operating empty weight increases by $0.4\,\%$ primarily due to the additional cabin air compressors. The electrified ECS architecture eliminates engine bleed air offtake and improves overall energy efficiency. The electric ECS consuming engine shaft power is predicted to have a fuel saving of $3.1\,\%$ and an overall energy saving of $3.3\,\%$ over a range of $180\,\mathrm{nmi}$. The electric ECS powered by the main battery is slightly less advantageous with a fuel saving of $2.6\,\%$ and a total energy saving of $3.0\,\%$ due to loss in the additional power conversion during in-flight recharging. Meanwhile, both electrified ECS architectures show a small range degradation up to $5\,\mathrm{nmi}$. Avenues of future work include a more comprehensive vehicle-level study considering the electrification of other secondary power subsystems and a propulsion-level and/or vehicle-level re-optimization to retain the baseline range capability.

Acknowledgment

The authors would like to thank NASA for their support of this effort under Contract Number 80LAR23DA003, especially Gaudy Bezos-O'Connor, Ralph Jansen, and Fayette Collier.

References

[1] S. Sahoo, X. Zhao, and K. Kyprianidis, "A review of concepts, benefits, and challenges for future electrical propulsion-based aircraft," *Aerospace*, vol. 7, no. 4, 2020.

[2] B. J. Brelje and J. R. Martins, "Electric, hybrid, and turboelectric fixed-wing aircraft: A review of concepts, models, and design approaches," *Progress in Aerospace Sciences*, vol. 104, pp. 1–19, 2019.

[3] Y. Cai, J. Xie, C. L. Pastra, N. R. Ndifor, A. M. Kehler, and D. Mavris, "Parametric mission performance assessment of regional turboprop aircraft retrofitted with hybrid electric propulsion," in *AIAA AVIATION FORUM AND ASCEND 2024*. American Institute of Aeronautics and Astronautics, Jul. 2024.

[4] G. Cinar, E. Garcia, and D. N. Mavris, "A framework for electrified propulsion architecture and operation analysis," *Aircraft Engineering and Aerospace Technology*, vol. 92, no. 5, pp. 675–684, 2020.

[5] D. Jimenez, E. Valencia, A. Herrera, E. Cando, and M. Pozo, "Evaluation of series and parallel hybrid propulsion systems for uavs implementing distributed propulsion architectures," *Aerospace*, vol. 9, no. 2, p. 63, 2022.

[6] F. Gaspari, L. Trainelli, A. Rolando, and I. Perkon, "Concept of modular architecture for hybrid electric propulsion of aircraft," *Mahepa, Nov*, 2017.

[7] I. Chakraborty, "Subsystem architecture sizing and analysis for aircraft conceptual design," Ph.D. dissertation, Georgia Institute of Technology, Nov. 2015.

[8] J. Xie, M. V. Bendarkar, Y. Cai, and D. N. Mavris, "Revisiting "critical-engine-inoperative" conditions for distributed hybrid-electric aircraft," in *AIAA AVIATION 2023 Forum*. American Institute of Aeronautics and Astronautics, Jun. 2023.

[9] I. Pérez-Grande and T. J. Leo, "Optimization of a commercial aircraft environmental control system," *Applied thermal engineering*, vol. 22, no. 17, pp. 1885–1904, 2002.

[10] M. Dechow and C. Nurcombe, "Aircraft environmental control systems," *Air quality in airplane cabins and similar enclosed spaces*, pp. 3–24, 2005.

[11] J. C. Ordonez and A. Bejan, "Minimum power requirement for environmental control of aircraft," *Energy*, vol. 28, no. 12, pp. 1183–1202, 2003.

[12] FAA, "Pressurization, ventilation and oxygen systems assessment for subsonic flight including high altitude operation," 1996. [Online]. Available: https://www.faa.gov/regulations_policies/advisory_circulars/index.cfm/go/document.information/documentid/22648

[13] *Systems 42 & 72-600*, ATR Product Support & Services, Jun. 2012.

[14] C. Müller, D. Scholz, and T. Giese, "Dynamic simulation of innovative aircraft air conditioning," in *1st CEAS European air and space conference*. German Society for Aeronautics and Astronautics, 2007, pp. 869–878.

[15] Y. Cai, "Multi-mission sizing and analysis framework for aircraft and subsystem architectures with electrified propulsion systems," Ph.D. dissertation, Georgia Institute of Technology, May 2023.

[16] D. P. Wells, B. L. Horvath, and L. A. McCullers, "The flight optimization system weights estimation method," NASA, Tech. Rep., Jun. 2017.

[17] R. C. Feagin and W. D. Morrison, "Delta method, an empirical drag buildup technique," NASA, Tech. Rep., Dec. 1978. [Online]. Available: https://ntrs.nasa.gov/citations/19790009630

[18] G. E. Tagge, L. A. Irish, and A. Bailey, "Systems study for an integrated digital/electric aircraft (idea)," BOEING COMMERCIAL AIRPLANE CO SEATTLE WA, techreport NASA-CR-3840 19850007405, Jan. 1985. [Online]. Available: https://ntrs.nasa.gov/citations/19850007405

[19] C. L. Pastra, C. Hall, G. Cinar, J. Gladin, and D. N. Mavris, "Specific power and efficiency projections of electric machines and circuit protection exploration for aircraft applications," in *2022 IEEE Transportation Electrification Conference & Expo (ITEC)*. IEEE, Jun. 2022.

[20] C. Hall, C. L. Pastra, A. Burrell, J. Gladin, and D. N. Mavris, "Projecting power converter specific power through 2050 for aerospace applications," in *2022 IEEE Transportation Electrification Conference & Expo (ITEC)*. IEEE, Jun. 2022.

[21] Y. Cai, C. L. Pastra, J. Xie, J. K. Thind, M. M. Monjon, J. C. Gladin, and D. N. Mavris, "System-level trade study of hybrid parallel propulsion architectures on future regional and thin haul turboprop aircraft," in *AIAA SCITECH 2023 Forum*. American Institute of Aeronautics and Astronautics, Jan. 2023.

[22] J. K. Lytle, "The numerical propulsion system simulation: An overview," National Aeronautics and Space Administration, Glenn Research Center, Cleveland, OH, techreport NASA/TM-2000-209915, Jun. 2000. [Online]. Available: https://ntrs.nasa.gov/citations/20000063377

[23] A. M. Kehler, Y. Cai, and D. Mavris, "Power management optimization of off-design missions for a sized hybrid-electric turboprop aircraft," in *AIAA AVIATION FORUM AND ASCEND 2024*. American Institute of Aeronautics and Astronautics, Jul. 2024.